Department of Physics and Astronomy
University of Heidelberg

Bachelor Thesis in Physics
submitted by

Richard Kaiser

born in Mannheim (Germany)

2017

Mesurement of the branching fraction of the rare decay of $D^{*0} \to D^0 e^- e^+$ at the LHCb experiment

This Bachelor Thesis has been carried out by Richard Kaiser at the
Physikalisches Institut in Heidelberg
under the supervision of
Prof. Dr. Stephanie Hansmann-Menzemer

Zusammenfassung

In dieser Arbeit wird ein oberes Limit des Verzweigungsverhältnises des seltenen Zerfalls $D^{*0} \to D^0 e^- e^+$ bestimmt. Die genutzten Daten stammen aus der im Jahre 2016 am LHCb Experiment aufgenommen Daten der Proton-Proton-Stöße. Die Schwerpunktsenergie betrug 13 TeV und die integrierte Luminosität entspricht 1.55 fb^{-1}. Der Zerfall $D^{*0} \to D^0 e^- e^+$ wurde untersucht und eine Signifikanz von 1.3σ wurde für die gefundenen Anzahl an rekonstruierten D^{*0} gefunden. Aus diesem Grund wurde ein oberes Limit bestimmt, welches zu 48 ± 2 rekonstruierten D^{*0} als oberes Limit führt. Das Limit für das Verzweigungsverhältnis wurde dann bestimmt zu

$$\mathcal{B}(D^{*0} \to D^0 e^- e^+) < (2.52 \pm 0.05_{stat.} \pm 0.12_{syst.}) \cdot 10^{-3}$$

bei einem Confidence Level von 95%.

Abstract

This Thesis presents an upper limit of the branching fraction for the rare decay of $D^{*0} \to D^0 e^- e^+$. The used data was recorded in 2016 on the LHCb experiment on proton-proton collisions,with a center of mass energy of 13 TeV and an integrated luminosity of 1.55 fb^{-1}. The goal was to estimate a background source for further analysis of Dark Photons in this channel. The decay $D^{*0} \to D^0 e^- e^+$ is studied and a significance of 1.3σ was found for the reconstructed events. Therefore the branching fraction is estimated with an upper limit according to a profile likelihood corresponding to be 48 ± 2 of reconstructed D^{*0}. The branching fraction is measured to be

$$\mathcal{B}(D^{*0} \to D^0 e^- e^+) < (2.52 \pm 0.05_{stat.} \pm 0.12_{syst.}) \cdot 10^{-3}$$

at a confidence level of 95%.

Contents

1 Introduction

The aim of particle physics is to find a correct description of matter and its interaction. Currently with the discovery of the Higgs boson the last missing piece of the Standard Model is finally observed. But particle physics is now not nearly complete understood and as Einstein said
"The fairest thing we can experience is the mysterious. It is the fundamental emotion which stands at the cradle of true art and true science." [1]
physicists will not rest on this triumph since there are still open questions which might be answered by physics beyond the Standard Model. One big open question in Physics is the Dark Matter, it is known to exist due to its Gravitational interaction on a cosmic scale since 1922[1]. But the Dark Matter remains dark for our means of observing Matter till today. But with upcoming detector upgrades at the LHC and the detection of Gravitational Waves in 2015 [3] major improvements in this field can be expected.

One way to search for Dark Matter is to use the Large Hadron Collider (LHC) at CERN. The LHC is a particle accelerator which uses either protons or lead-ions. In this Thesis the proton-proton collision are studied. The generated particles from the collision of the protons can either be measured directly for long living particles (such as electrons or pions) or by combining the information gathered from daughter particles. The LHCb experiment is one of four large experiments of the LHC and focuses on the study of B hadron physics. Data accuired by the LHCb in the year 2016 was used in this thesis. To search for a Dark Photon as opposed by this thesis a rare decay of a $D^*(2007)^0 \to D^0\gamma$ is studied. In theory the Photon would mix with a Dark Photon. The only observable difference would be a shorter lifetime than a photon and a the four-momenta.

In this study a background for further searches in this decay is provided, since the branching fraction of the $D^{*0} \to D^0 e^- e^+$ is estimated with an upper limit approach. At first the basics concept of particle physics is

[1] First suggestion of Dark Matter by Jacobus Kapteyn in the year 1922. In 1933 The name "dunkle Materie" (Dark Matter) was introduced by Fritz Zwicky [2]

explained in Section 2. afterward the experimental setup is discussed in Section 3. As next step the selection of the signal takes place in the main part of this thesis the Analysis Section 4. Here the background is seperated in various steps. The begin takes place with stripping and preselection cuts. Afterwards a multivariate analysis is made with corrected simulated samples. At last the signal is fitted, but with a significance of 1.3σ for the resulting number of reconstructed events, an upper limit approximation is made. The branching fraction is then calculated using this upper limit in Section 5. After addressing the systematic uncertainties in Section 6 the result is presented in Section 7.

2 Theory

This chapter shortly explains the Standard Model which is needed to understand the concept of this Thesis. First it will give a short overview of the Standard Model (SM) of particle physics and then a brief explanation about Dark Photons and the observed decay channel. For a more detailed description and further information it is referred to [4].

2.1 Standard Model

The Standard Model is a Quantum Field Theory which describes Particles as a field and interaction between particles with gauge bosons. In the SM there are fermions and bosons. Fermions have an half integer spin and thus obey the Pauli Principle and follow the Fermi-Dirac-Statistic. bosons have an integer Spin and follow the Bose-Einstein-statistic. There are five gauge bosons, twelve Fermions and the Higgs boson. Fermions are further divided into quarks and leptons, each with their respective antiparticle. Antiparticles are equal to their associated particle but with an opposite charge. The six quarks (up, down, charm, strange, top, bottom) and the six leptons (electron, electron neutrino, muon, muon neutrino , tau, tau neutrino) are distinguished by their means of interaction (see Figure 2.1). Neutrinos have no electric or color charge therefore only interact via the weak interaction and thus are hard to detect. The charged leptons (electron, muon, tau) interact also with the weak interaction but due to their electric charge also with the electromagnetic interaction. Quarks additionally carry a color charge (red, green, blue, anti-red, anti-green, anti-blue) and interact mostly with the strong interaction but also with the electromagnetic and the weak interaction.

Weak Interaction The weak interaction couples with all fermions. The mediator particles of the weak interaction (W^{+-}, Z) have a non zero-mass (see 2.1). This suppresses the interaction probability drastically and decreases the lifetime of the gauge Bosons and electroweak decays. As consequence the interaction Range is therfore limited to about $10^{-3} fm$.

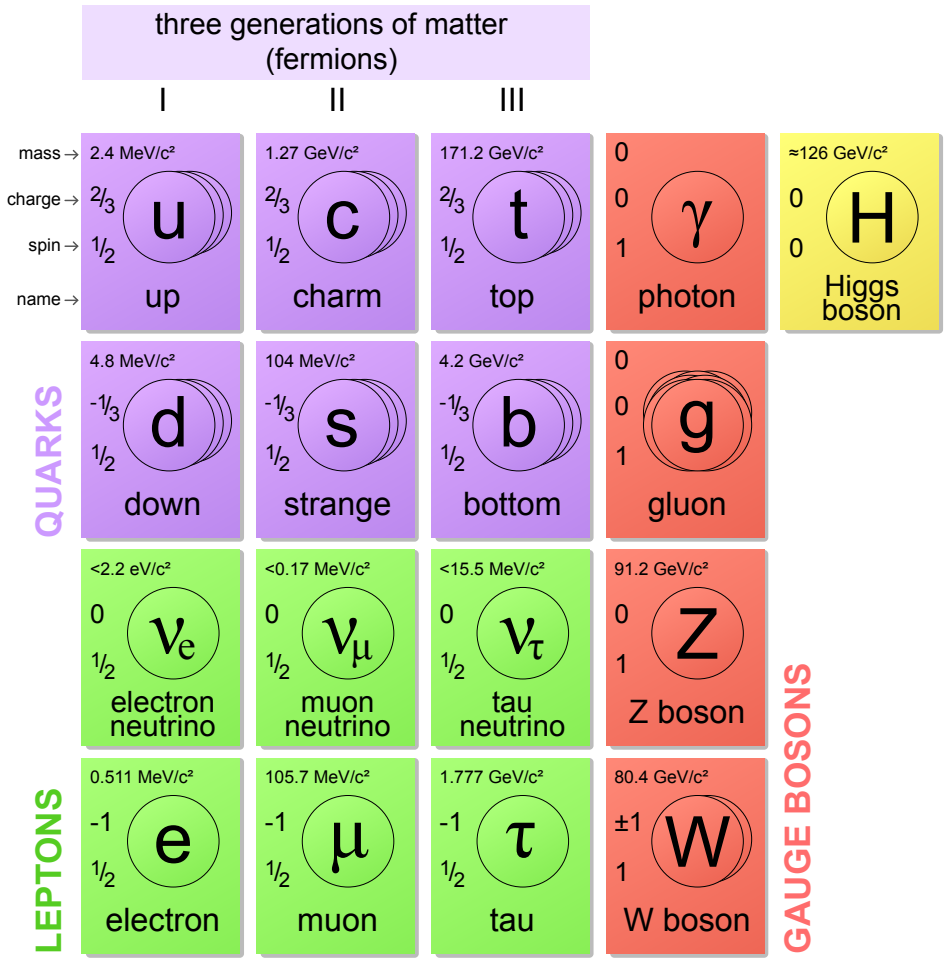

Figure 2.1: Standard Model of particle physics from [5]

Electromagnetic Interaction The electromagnetic interaction couples on all charged fermions. The mediator is the Photon. The range of interaction is infinite but the strength decreases with distance.

Strong Interaction The strong interaction couples via gluons and only with quarks and gluons since those are the only ones with color charge. Gluons themselves have a color charge of red-antiblue or green-antiblue or a superposition of both, in total 8 different gluons. But quarks only form bound states (Hadrons), these must be color neutral. Baryons are a neutral bunch of three quarks with three different colors either blue,green

Boson	Mass$[\frac{GeV}{c^2}]$	Spin	Mediator
Photon (γ)	0	1	electromagnetic interaction
W^{+-}	80.4	1	weak interaction
Z	91.2	1	weak interaction
gluon (g)	0	1	strong interaction
Higgs boson	125.7	0	Higgs field

Table 2.1: gauge bosons from [4, 6]

and red or anti-blue, anti-green and anti-red. Particles with two quarks (color and anticolor) are called mesons. The existence of hadrons with four and five quarks (Tetra- and Pentaquark) was measured by the LHCb, see [6] and [7] respectively.

Higgs Field At last there is the Higgs field and the Higgs boson. It is responsible for the masses of the fermions and gauge bosons. The Higgs has a spin and electric charge of 0. It was Measured in 2012 by the LHC [8] and was the last missing particle in the SM to be observed.

2.2 Dark Photons

In this thesis the main goal is to observe a Dark photon. To achieve this we observe the decays of a $D^*(2007)^0 \to D^0\gamma(\to e^-e^+))$ and $D^*(2007)^0 \to D^0e^-e^+$ as seen in 2.2. Assuming that instead of a Photon there could be a Dark Photon (DP) emitted which has a non-zero mass and short lifetime as published by [9]. In this thesis the Branching Fraction of $D^*(2007)^0 \to D^0e^-e^+$ will be determined. This serves as background for further searches of a Dark Photon in this channel.

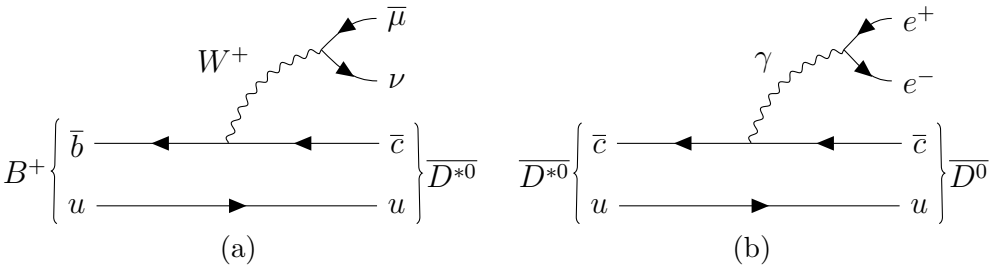

Figure 2.2: Feynman graph of $B^+ \to D^*(2007)^0 \mu\nu$ (a) and $D^{*0} \to D^0\gamma$ (b). For the graph on the right a decay with a virtual photon is regarded as the decay from$D^{*0} \to D^0 e^- e^+$.

3 The LHCb Experiment

This chapter gives an outline of the Large Hadron Collider (LHC) and a detailed discussion about the Large Hadron Collider beauty (LHCb) experiment which is one of seven large Experiments at the European Organization for Nuclear Research (CERN). The goal of the LHCb is to look for new physics in B-meson decays. First the LHC will be briefly discussed and then the LHCb experiment and its detectors in detail.

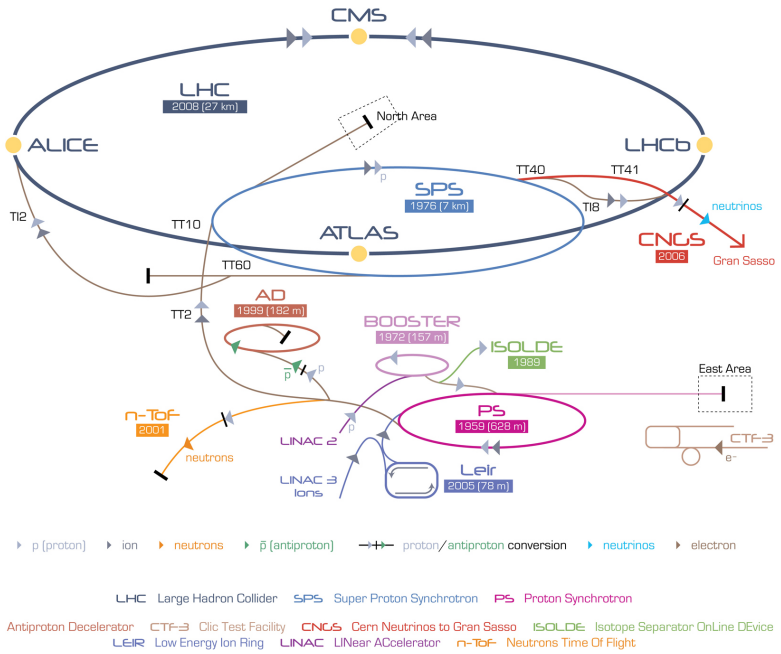

Figure 3.1: Topography of the LHC as seen from above [10]. All major Experiments are shown as well as the whole LHC complex with all its Particle accelerators

3.1 The Large Hadron Collider

The Large Hadron Collider (LHC) is the currently most powerful particle accelerator in the world. It is located near Geneva, Switzerland and lies in

a tunnel of 27 kilometers circumference beneath the France-Switzerland border. Two proton bunches are accelerated and collided. It has 7 experiments with the 4 large Experiments ATLAS, CMS, LHCb and Alice were the beams collide and three smaller ones LHCf, TOTEM and MoEDAL. ATLAS stands for A Toroidal LHC ApparatuS and together with the Compact Muon Solenoid (CMS) search for direct production of heavy new particles, so-called New Physics beyond the Standard Model. The Higgs boson was detected by both of these detectors. LHCb is a forward arm spectrometer and as the Name suggests specialized in b/hadrons and b physics. Alice (A Large Ion Collider Experiment) is used to study heavy ion collision of Pb-Pb pairs with a centre-of-mass energy of around 2.76 TeV. The LHCf (Large Hadron Collider forward) experiment is designed for astroparticle physics and as the name suggests in forward direction of the beam almost inline of the beam. It coexists with the larger Experiment ATLAS and shares the same Interaction point. TOTEM (TOTal Elastic and diffractive cross section Measurement) is specialized in cross sections and elastic scattering and shares the interaction Point with the CMS. Lastly there is the MoEDAL (Monopole and Exotics Detector At the LHC) which searches for magnetic monopoles or dyons and other highly ionizing particles. It shares the intersection point with the LHCb experiment.

3.2 The LHCb

The LHCb detector is a single arm forward spectrometer as seen in Figure 3.2. The LHCb is positioned at point 8 at the LHC. Since b hadrons are heavily boosted in one direction this layout is optimal for detecting and observing b-hadrons and their daughter particles. The aim of the LHCb experiment is to perform indirect searches for New Physics in precision measurements of b and c hadron decays. The LHCb consists of several detectors for Particle Identification and Track reconstruction and a Magnet to bend charged Particles for measuring their momentum.

3.2.1 Magnet

The LHCb has a Magnet between its TT and T1. The magnet consists of two coils weighing 27 tonnes. It generates a 4Tm integrated magnetic Field along a span of 10m. The charged particles are bend only in the x direction with z being in direction of the beam. The bend of the particles allows a measurement of the momentum of the particle. In some cases the Particles are bend out of region for the following downstream detectors.

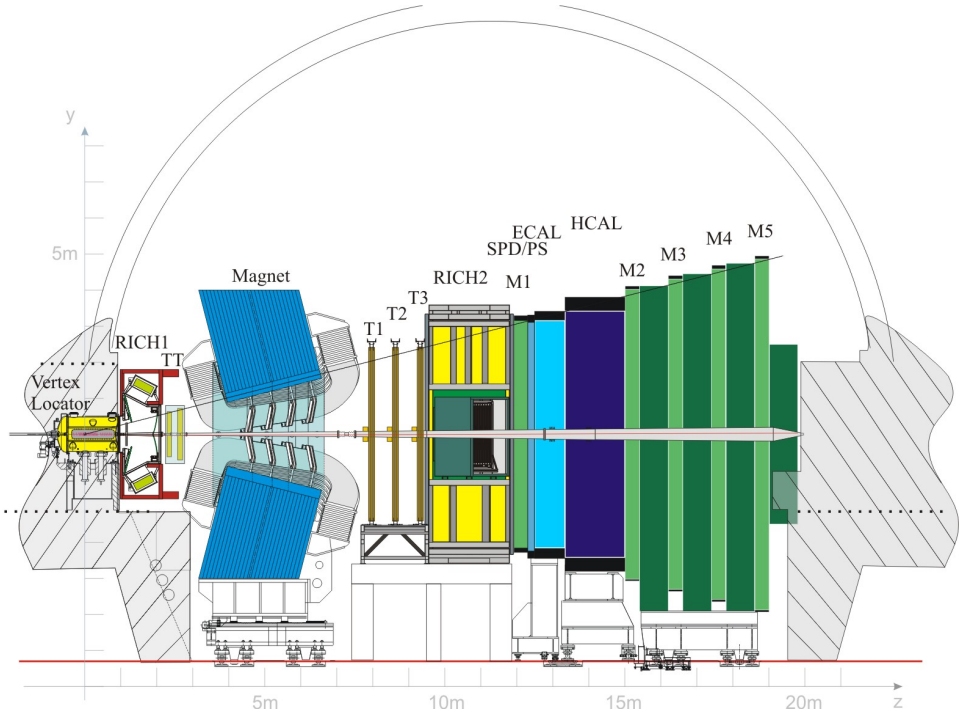

Figure 3.2: LHCb Crosssection from [11]

The track of those particles are called Upstream Tracks whereas for particles going through the whole detector they are called Long Tracks, as seen in figure 3.3. The Magnet can change its magnetic field in two states, MagUp and MagDown. This is used to eliminate detector asymmetries.

3.2.2 Vertex Reconstruction

Vertex Locator Inside the Vertex Locator (VELO) the collision of the protons takes place. Many tracks will originate here in the so-called Primary Vertex which describes the location of the proton-proton collision. But the B mesons lives for a short while and can be distinguished from the Primary Vertex, the so-called Secondary Vertex. The VELO consist of 21 half circle pairs of detectors which are located around the beam pipe. For protection of the detector the pairs can be moved away from the beam pipe when the LHC is starting up.

Tracking Stations There are two Tracking Stations, TT before the magnet and T1-T3 afterwards. The TT consists of two seperate modules with 2 layers each. The T1-T3 stations consists of four layers. The inner Layers

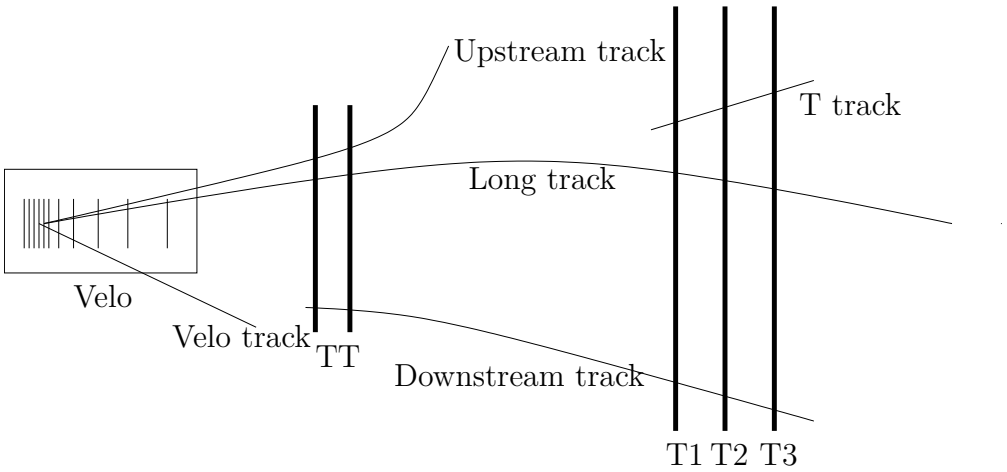

Figure 3.3: View of the different types of Tracks at the LHCb experiment. Taken from [12]

of all Tracking Stations are tilted by +5 degrees with the beam as rotary axis. For detection two techniques are used, the silicon tracker (ST) and the outer tracker (OT). The ST uses silicon microstrip detectors with a spatial resolution of roughly $50\mu m$. The TT consists solely of the ST and covers the full detector acceptance. For the T1-T3 stations only the inner area is made from the ST where as the outer region uses the straw tubes of the OT.

3.2.3 Ring Imaging Cherenkov Detectors

For Particle Identification there are two Ring Imaging Cherenkov detectors (RICH) installed in LHCb. The detectors measure the emission of the Cherenkov Radiation. This Radiation is emitted if a charged particle is faster than the speed of light in a certain medium, similar to the sonic boom when breaking the sound barrier. The shape of the cone than depicts a particles velocity. Combining the information gathered for the Trajectory from the Tracking Stations and the VELO the mass and charge of the particle can be obtained. It is mostly used for distinguishing pions, kaons and protons since those are mostly produced from a B-meson decay. RICH1 is positioned upstream of the magnet and between VELO and TT. It measures particles with momenta ranging from 10 GeV/c to 65 GeV/c. RICH2 is Upstream located behind the magnet and limited to a low angle region and designated for high-momentum particles. It covers a momentum range of 15 GeV/c to 100 GeV/c.

3.2.4 Calorimeters

The calorimeters in the LHCb experiment are used to determine the position and energy of hadrons, electrons and protons. All four calorimeters are located downstream of RICH2. They are briefly explained in the following.

Scintillating Pad Detector The first layer of calorimeters is the Scintillating Pad Detector (SPD). It distinguishes charged from neutral particles, which is crucial since it provides a trigger for charged particles.

Pre-Shower Detector Second is the Pre-Shower Detector (PS) located. A 15mm lead plate is sandwiched between the SPD and PS and causes electrons to shower. Since Hadrons have a larger Interaction range they do not shower here. It uses scintillating pads for the detection of the showers.

Electromagnetic Calorimeter The electromagnetic calorimeter (ECAL) is using a shashlik technology by using several layers of absorption material (2 mm lead) and scintillating plates. Combined resulting in a total thickness of 42 cm which is equal to 25 radiation lengths. Through Bremsstrahlung and pair production electrons and photons shower in the ECAL. The resulting charged particles scintillate in the scintillating plates and registered in photomultiplier's. The energy resolution of the ECAL is $\sigma_E/E = \frac{10\%}{\sqrt{E}} \oplus 1\%$ with E in GeV.

Hadronic Calorimeter At last there is the hadronic calorimeter (HCAL) which works similarly to the ECAL. Iron is used as absorption material with a length of 5.6 interaction lengths. As the name suggests its purpose is to detect hadrons. In the HCAL hadronic showers are produced. The charged particles are then detected following the same principle as the ECAL. The Energy resolution of the HCAL is $\sigma_E/E = \frac{(69\pm5)\%}{\sqrt{E}} \oplus (9 \pm 2)\%$ for E in GeV.

3.2.5 Muon Stations

There are five muon stations (M1-M5) in use at the LHCb experiment. They are located at the far end of the detector (M2-M5) and M1 is located in front of the SPD to improve transverse momentum measurements. To reduce hadronic background the downstream stations (M2 - M5) are seperated by a 80 cm thick iron plate. The detectors are optimized for

speed since they must provide Level-0 Trigger information and muon identification for the high-level-trigger (HLT).

3.2.6 Particle Identification

Finally with all the information combined in the RICH detectors, the calorimeters and the muon stations a likelihood function is generated. The difference of this likelihood function compares the likelihood of a given particle with the likelihood of a pion. The logarithmic function of this difference is then referred to as PIDX where X is the particle hypothesis and classification with either a kaon, proton, muon or pion.

4 Analysis

This chapter describes the used Analysis with the used datasets and the used selections to gain a clear signal. First loose cuts are applied to reduce the data size, then a comparison of the simulated sample is done. Afterwards a Multivariate Analysis is used to reduce kinematic and combinatorial background even further. Finally the fit is described, which is used to determine the branching fraction .

4.1 Strategy

In this thesis the decay

$$D^{*0} \to D^0 e^- e^+$$

is studied and the branching fraction determined with regards to the control channel

$$D^* \to D^0 \gamma (\to e^- e^+).$$

In both channels they decay to $D^0 \to K^+ \pi^-$. Since both end products are the same only the location and invariant mass can be used to differentiate both. The reason a semileptonic decay from$B^+ \to D^*(2007)^0 \mu\nu$ was studied is that with the μ an easy Trigger is guaranteed. But as a Downside of this decay are the low Energy electrons with a combined Energy of around 142 MeV (difference of the masses from $D^*(2007)$ and D^0).
The strategy to minimize the background while maintaining most of the signal is as followed.

1. **Stripping**. Stripping defines a loose preselection generally created by the LHCb collaboration to minimize computational power in further analysis.

2. **Preselection**. Cuts are applied to the datasample to reduce background and make the desired decay visible. See Section 4.3 for more Information.

3. **Monte Carlo Calibration**. Here the simulated Monte Carlo sample is corrected to describe the used data sample correctly. This is needed since the Monte Carlo sample is used to as signal source of

a Multivariate Analysis to the selection as well as to calculate the corresponding efficiencies.

4. **Selection**. The signal is further enhanced by using a Multivariate Analysis (see Section 4.5). The Multivariate Analysis is trained on data and optimized with simulated data.

5. **Fitting**. The signal of both decays is now fitted with an unbinned likelihood fit to extract the signal yields. The signal yields are then used to determine the branching fraction.

4.2 Data sets

4.2.1 Definiton of Detector Variables

There are many variables available for each measured particle in the LHCb experiment. All used variables in this thesis are therefore shortly explained.

Mass The invariant mass of a particle can be obtained by taking the squareroot of its four-momentum (p)

$$m = \sqrt{p^2}.$$

Transverse Momentum The transverse momentum (p_T) is the momentum transversal to the beam (z-axis).

$$p_T = \sqrt{p_x^2 + p_y^2}$$

B Corrected Mass The obtained mass of the B meson is off from its origin since a neutrino is generated in this decay. Neutrinos can not be measured by the LHCb and therfore distort the reconstruction of the B meson mass. The B corrected mass (BPVCORRM) is obtained by

$$BPVCORRM = \sqrt{m_{vis}^2 + PT_{vis}^2} + PT_{vis}$$

where vis means the mass or PT of all visible daughter particles.

Impact Parameter The Impact Parameter (IP) is the minimal distance between the primary vertex and the reconstructed trajectory of the observed particle, as shown in figure 4.1a. The χ^2 of the Impact Parameter is the difference of the χ^2 of the fit of the Primary Vertex before and after the track is added.

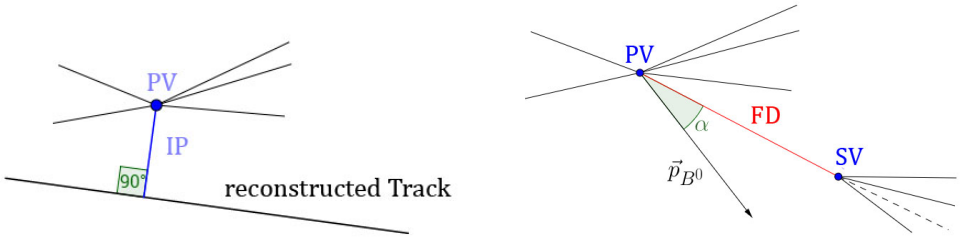

(a) Representation of the impact parameter.(b) The flight distance and direction angle are shown.

Figure 4.1: Visualization of the variables flight distance, direction angle and impact parameter, taken from [13]. The direction angle is the cosine of α.

Particle Identification The PID variable is explained in chapter 3.2.6.

Vertex and Track quality The $vertex_{\chi^2}$ and $track_{\chi^2}$ are defined as the quality of the vertex and track, respectively. They are obtained by their fit model.

Flight Distance The flight distance (FD) is the distance the particle is travelled between the primary and secondary vertex, as shown in figure 4.1b.

Direction Angle The direction angle (DIRA) is the cosine of the angle between the flight direction and the momentum of the mother particle. It can be seen in figure 4.1b

Ghost probability The Ghost probability describes the probability of a particle to be not from an other particle or from combining hits of several particles. They are called ghosts.

4.2.2 Preparation of the Data Sets

The datasets used in this thesis are from Run2(2016) of the LHCb and have an integrated Luminosity of 1.55 fb^{-1} and center-of-mass energy of 13 TeV. All data sets use the long and upstream tracks. There are in total three data sets used.

First there is the Data set which describes the main data channel now referred to as data. It is form the Deacy of $B^+ \to D^{*0}\mu\nu$ and the preferred daughter decay in this Dataset is $D^{*0} \to D^0 e^- e^+$.

The second is the control channel which is used for a later reweight of the simulated sample. It is referred to as control channel in this thesis. And the preferred decay in this Channel is $D^{*0} \to D^0\gamma(\to e^- e^+)$.

At last is the Monte Carlo Sample it is the only sample from the 2015 Run of the LHC. The Monte Carlo sample also centers the $B^+ \to D^{*0}\mu\nu$ decay with the $D^{*0} \to D^0 \to e^- e^+$ decay. A Monte Carlo sample is a simulated sample. It uses random numbers to generate an outcome. It helps to understand and obtain certain Information that is hard to see in real data.It can be greatly used to observe cuts and validate fit parameters since the background in Monte Carlo is understood.

To reduce the amount of recorded data, a so-called stripping is applied after measuring the data. Only events going through the selection are considered in the datasets and therefor in this thesis. For this analysis the stripping line Stripping22 was used with its parameters shown in table 4.1. As required step the Monte Carlo sample is truthmatched after stripping. Truthmatching describes a process only available in simulated samples. Since in a simulation the identity of a particle is known in every step of simulation a misidentified particle can easily be ignored by only looking at corrected events.

Candidate	Selection
Muon	$Track\chi^2/ndof < 3$
	$Minimum(IP\chi^2) > 9$
	$p > 6GeV$
	$p_T > 1.0GeV$
	$PID_\mu > 0$
Charm hadron (CH)	$Vertex\chi^2/ndof < 6$
	$FD\chi^2 > 25$
	$DIRA > 0.99$
Charm hadron daughter	$Track\chi^2/ndof < 3$
	$Minimum(IP\chi^2) > 4$
	$p > 2GeV$
	$p_T > 0.25GeV$
Proton	$p > 8GeV$
	$PID_p > 0$
Kaon	$p > 5GeV$
	$PID_K > -2$
Pion	$PID_K < 20$
B^+	$Vertex\chi^2/ndof < 3$
	$DIRA > 0.999$
	z(charm)-z(b)
	$2 < \eta < 5$
	$2.2GeV < CH_m + \mu_m < 8.0GeV$
	$NLongTracks < 250$

Table 4.1: Stripping cuts applied for Stripping22.

4.3 Preselection

A preselection cut is loose cut on a variable in order to maintain the signal events and removing as much background events as possible. Therefore preselection cuts should be efficient and only reduce signal significantly less compared to the background. To test this the cuts were applied on the MC sample and if the loss of signal is acceptable the cut is applied. All used cuts for preselection after Stripping are given in table 4.2. As extra cut on the control channel a cut for $m_gamma < 10\ MeV$ and for the data channel a cut for $m_gamma > 20\ MeV$ was made, this guarantees that for the control channel only Photons are regarded and for the data channel only the decay into two electrons is regarded.
The desired observed variable in this deacy is the mass difference of D^{*0} and D^0, now referred to as Δm. The difference of those two masses gives a sharper signal since variations in the D^0 mass would directly effect the D^{*0} mass reconstruction, and those are now eliminated. Befor applying the cut no clear peak can be seen. After applying the preselection it is clearly visible in figure 4.2 that two peaks can be seen, one at around 80 MeV and a larger one at around 140 MeV. The origin of the first one is unknown whereas the second one is the desired Peak of the mass difference at 142 MeV. On the data channel the Difference between before and after the preselection cut is visible but there is no clear spike evolving from it as in the control channel.

gamma	electrons	D^0
$Vertex^2_\chi < 5$	PIDe >0	$D^0\ Vertex_Z > B^+\ Vertex_Z$
PT > 400	PT > 100	1828 MeV < m < 1900 MeV
	GhostProb < 0.2	
	$IP\chi^2 > 4$	

Table 4.2: Cutvalues for the preselection on the datasets.

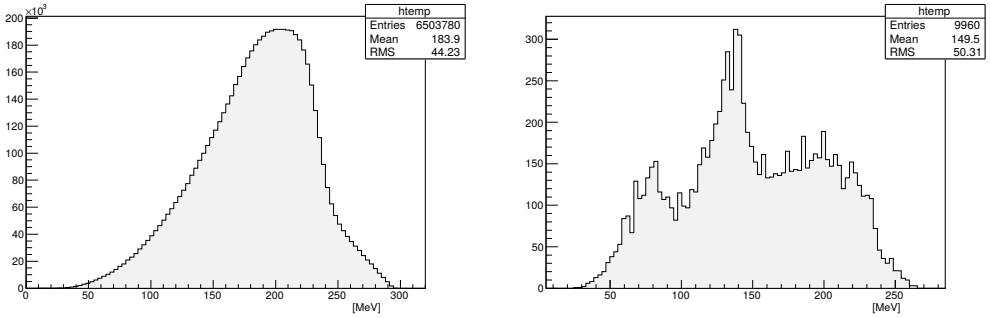

(a) Difference of the masses of D^{*0} and D^0 in the control channel data.

(b) Difference of the masses of D^{*0} and D^0 on the control channel data after preselection.

Figure 4.2: Comparison of the mass difference of D^{*0} and D^0 before (a) and after (b) the preselection on the control channel.

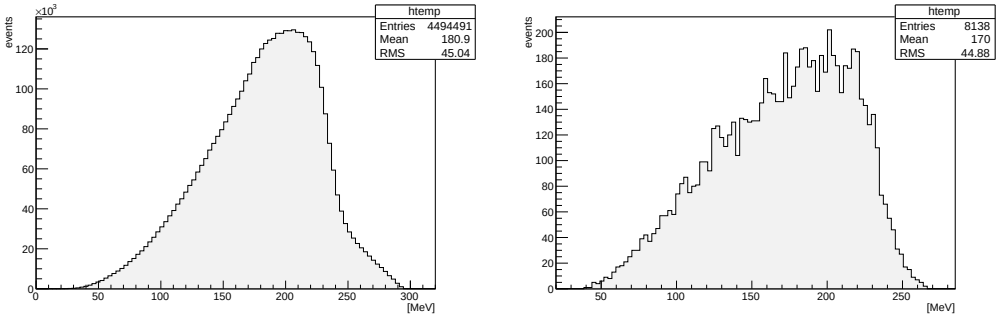

(a) Difference of the masses of D^{*0} and D^0 on the data channel.

(b) Difference of the masses of D^{*0} and D^0 on the data channel after preselection.

Figure 4.3: Comparison of the mass difference of D^{*0} and D^0 before (a) and after (b) the Preselection on the data channel.

4.4 Monte Carlo calibration

4.4.1 SWeighting Data

To establish a pure signal sample from data the *sPlot* technique is used. This is a statistical tool which uses discriminating variables, which are variables with knowledge of the distribution of background and signal. By using a fit which is then used to weight the candidates accordingly. If the sWeights are now applied to the data sample a clean signal distribution is obtained. For each candidate one sWeight is computed to the distribution of the discriminating variable. For further Information about sPlots see [14].

For this decay the discriminating variable is chosen to be the mass difference of D^{*0} and D^0 (Δm) as seen in figure 4.4. The Fit was made on the control channel with preselection as described in section 4.3. As signal Fit a Crystal Ball function [15] is used. The Crystal Ball function (CB) is a gaussian with an exponential tail. The tail is used for particles which loose energy in a radiative process or Bremsstrahlung. The CB has four parameters (α, n, μ, σ) and is defined as

$$CB(x;\alpha,n,\mu,\sigma) = N \cdot \begin{cases} exp(-\frac{(x-\mu)^2}{2\sigma^2}), & \text{for } \frac{x-\mu}{\sigma} > -\alpha \\ A \cdot (B - \frac{x-\mu}{\sigma})^{-n}, & \text{for } \frac{x-\mu}{\sigma} \leq -\alpha \end{cases}$$

with

$$\begin{aligned} A &= (\frac{n}{|\alpha|})^n \cdot exp(-\frac{|\alpha|^2}{2}), \\ B &= \frac{n}{|\alpha|} - |\alpha|, \\ N &= \frac{1}{\sigma(C+D)}, \\ C &= \frac{n}{|\alpha|} \cdot \frac{1}{n-a} \cdot exp(-\frac{|\alpha|^2}{2}), \\ D &= \sqrt{\frac{\pi}{2}} \cdot (1 + erf(\frac{|\alpha|}{\sqrt{2}})). \end{aligned}$$

where μ and σ are exactly like in a gaussian the mean and sigma, N is a normalization factor, α marks the transition between gaussian and tail and n defines the shape of the tail. The tail on the left is used to describe Bremsstrahlung coming from the electrons. As background function for

the fit two functions are used, one is a gaussian to describe the peak at around 80 MeV with unknown origin and the other one is a square root function (sqf) as follows.

$$sqf(x; a, b) = (x - b)^a \quad \text{for } x - b > 0$$

The square root function is necessary to describe the shape of the combinatorial background.
In Total ten parameters were used for the fit. Seven parameters come from the fit functions and three parameters are for the ratio of the three fit functions. The mean of the Crystall Ball was kept constant at 138 MeV for a better fit convergence .

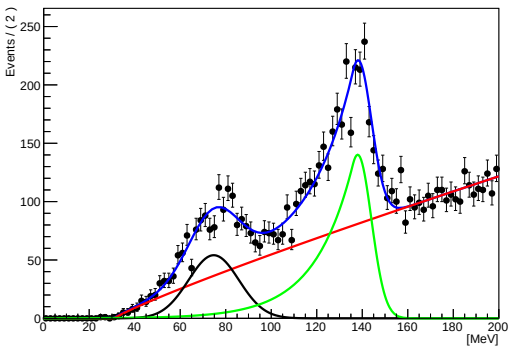

$$\begin{aligned}
\alpha_{CB} &= 0.356 \pm 0.033, \\
n_{CB} &= 99.9 \pm 9.9, \\
\sigma_{CB} &= 6.02 \pm 0.50, \\
\mu_{gaus} &= 74.7 \pm 0.8, \\
\sigma_{gaus} &= 11.1 \pm 0.9, \\
a_{sqf} &= 0.89 \pm 0.06, \\
b_{sqf} &= 31.0 \pm 0.7, \\
BG_{yield} &= 6183 \pm 121, \\
Sig_{yield} &= 1798 \pm 102, \\
Ratio &= 0.12 \pm 0.01.
\end{aligned}$$

Figure 4.4: Fit of the mass difference of D^{*0} and D^0 to determine the Sweights on the right and on the left the obtained fit parameter. Blue is the complete fit whereas green is the CB, black the gaussian and red the sqf.

4.4.2 Reweighting Monte Carlo

Comparing now the sweighted data with the Monte Carlo sample it is clearly seen that the values for B^+_PT and other PT Values are not the same see figure 4.5. The IPχ^2 values and the other values shown in the Appendix (A.1) are in good agreement with the data. The MC sample has to be reweighted to establish that there are no uncertainties

between both and to use it as a signal sample in the upcoming Multivariate Analysis. The reweight rakes into account the fraction of the Monte Carlo in regards to the control channel on the B^+_PT variable, in this case. It saves for every entry the fraction and then applies it in the reweight on all variables. Therefore a complete Agreement in the B^+_PT Variable should be achieved and good agreements in all other kinematic variables.

The data to test with is the sweighted data from the control channel of the previous section. After reweighting the MC is exactly like the dataset in the observed 16 variables (see Appendix A.1) except for μ_PIDmu and the maximum of the IPχ^2 of the electrons, both were not used in further Analysis. A second reweight to establish accordance for those two values could be done, due to time constraints.

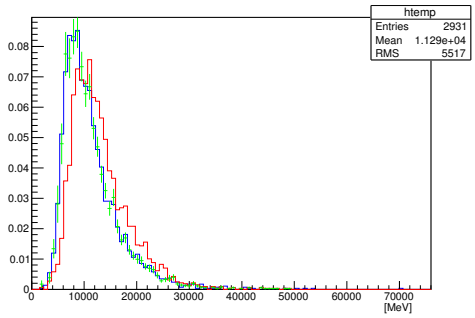

(a) B^+P_T

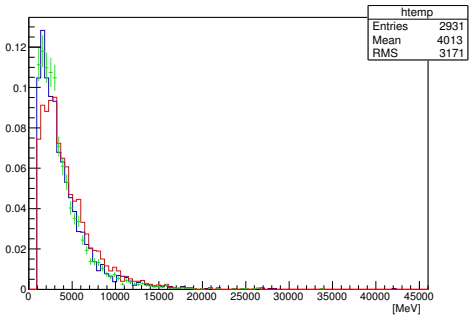

(b) μP_T

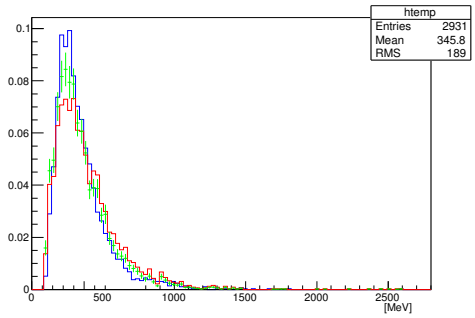

(c) e^+P_T

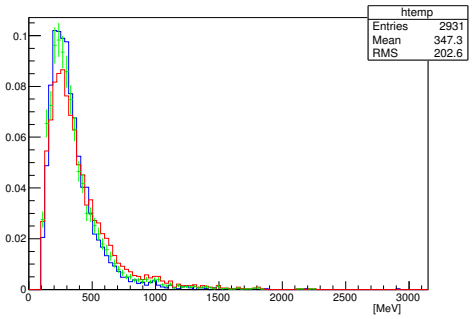

(d) e^-P_T

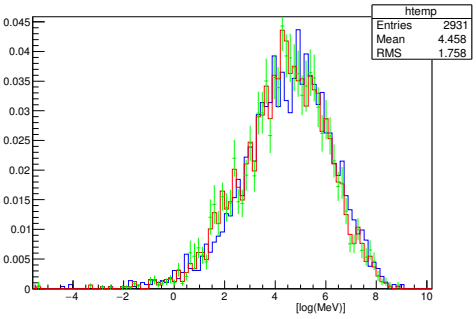

(e) $log(B^+IP\chi^2)$

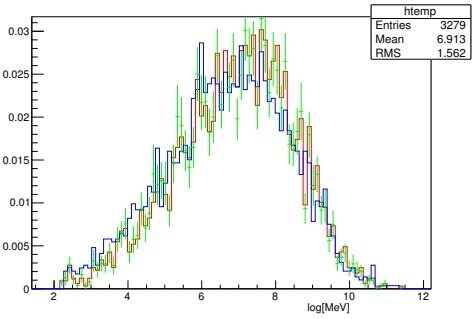

(f) $log(\mu IP\chi^2)$

Figure 4.5: Going from left to right the Distributions are the transverse momentum (P_T) for B^+, μ, e^+ and e^-. And the last two are the $log(IP\chi^2)$ of B^+ and μ. The Monte Carlo before reweighting is in blue and after reweighting in green. The sweighted data is in red. The difference in the Transverse Momentum variables is clearly visible.

4.5 Multivariate Analysis

To gain a pure signal sample with less background a Multivariate Analysis is used. In a Multivariate Analysis many variables will be analyzed simultaneously like the PT, Mass, Vertex etc. of a particle. This makes the cut more efficient and the separation power is significantly larger than multiple single cuts[1]. A Multivariate Analysis needs to be trained and tested before it can be used[2]. In training the Analysis gather the information for the cuts and variables and in testing the retrieved information is used. A Multivariate Analysis can overtrain. This means that the analysis gathers statistical fluctuation on training and applies those to the test sample which makes the result much worse and the analysis weak to fluctuations. As Multivariate Analysis Tool the Toolkit for Multivariate Analysis implemented in Root (TMVA [16]) is used.
For the analysis a Boosted Decision Tree (BDT) is used. A decision tree is a binary tree with decisions as nodes (see figure 4.6). On each node one variable is tested and than classified either signal or background like. An event therefore passes several nodes and comes to an end by a given stop parameter. The event is than either a signal event (+1) or a background event (-1). The desired values for the nodes are gathered by the decision tree in the training run and applied in testing. This results in a good seperation of signal and background, but to get a further increased separation power and to establish a statistical independence and minimizing statistical fluctuations the decision tree is boosted. It is not only once made and executed but several times, a forest of decision trees is made. In the forest the values for the nodes changes to minimize statistical fluctuations. In the end the results for each event are normalized and a continuous distribution is made between -1 and 1. Values which are in a previous BDT misclassified (e.g. a signal event is classified as background event) get a weight attached, therefore the next tree will be more sensitive to those misclassification of the tree before him. Values greater than zero are than regarded as signal like and less than zero as background like.
A combinatorial background sample has to be selected which in this case is made by using Bplus corrected mass grater than 6000 MeV as discriminating cut on the data. This is taken from the uncut data sample. The used Variables are shown in table 4.3 and figure 4.7 and are all gathered from

[1] As a single cut a one dimensional cut is meant. Which only applies to one variable in one dimension.

[2] For best results three statistical independent data should be used in a Multivariate Analysis. One for training, one for testing and the last one for using the Analysis.

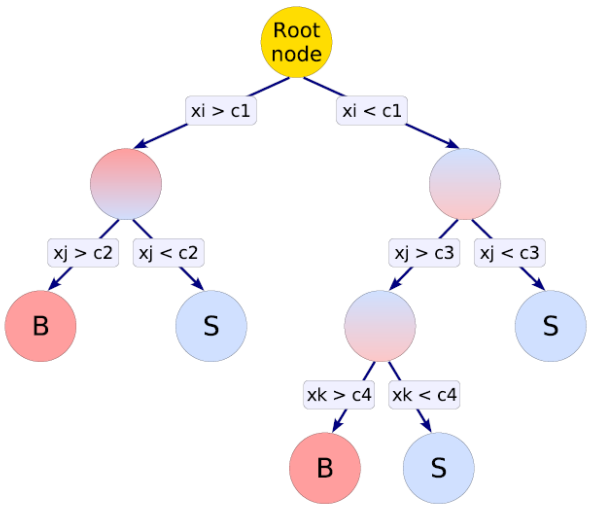

Figure 4.6: Schematic Overview of a decision tree. An event starts at the top (root) node and makes it way down through the nodes. The nodes define a binary decision and the event can only go left (background like) or right (signal like). The S and B defines the end state of the event, if it is signal or background. This image is taken from [16]

Bplus	electrons	μ
$Endvertex\chi^2$	PIDe	$\log(\mathrm{IP}\chi^2)$
PT	PT	PT
$\log(\mathrm{IP}\chi^2)$	GhostProb	

Table 4.3: Variables used in the Multivariate Analysis.

the kinematics of the decay. Great discrimination power can be seen for the PT values of all observed particles. Training and testing samples are combined in this case, and as signal sample the reweighted Monte Carlo is used. The BDT output in figure 4.8 shows a good response but a slight overtrain for the signal sample. This comes rather from the small Monte Carlo sample than from Overtraining as only a few Variables are used. As next step the BDT has to be used on the data and a optimal cut value must be found.

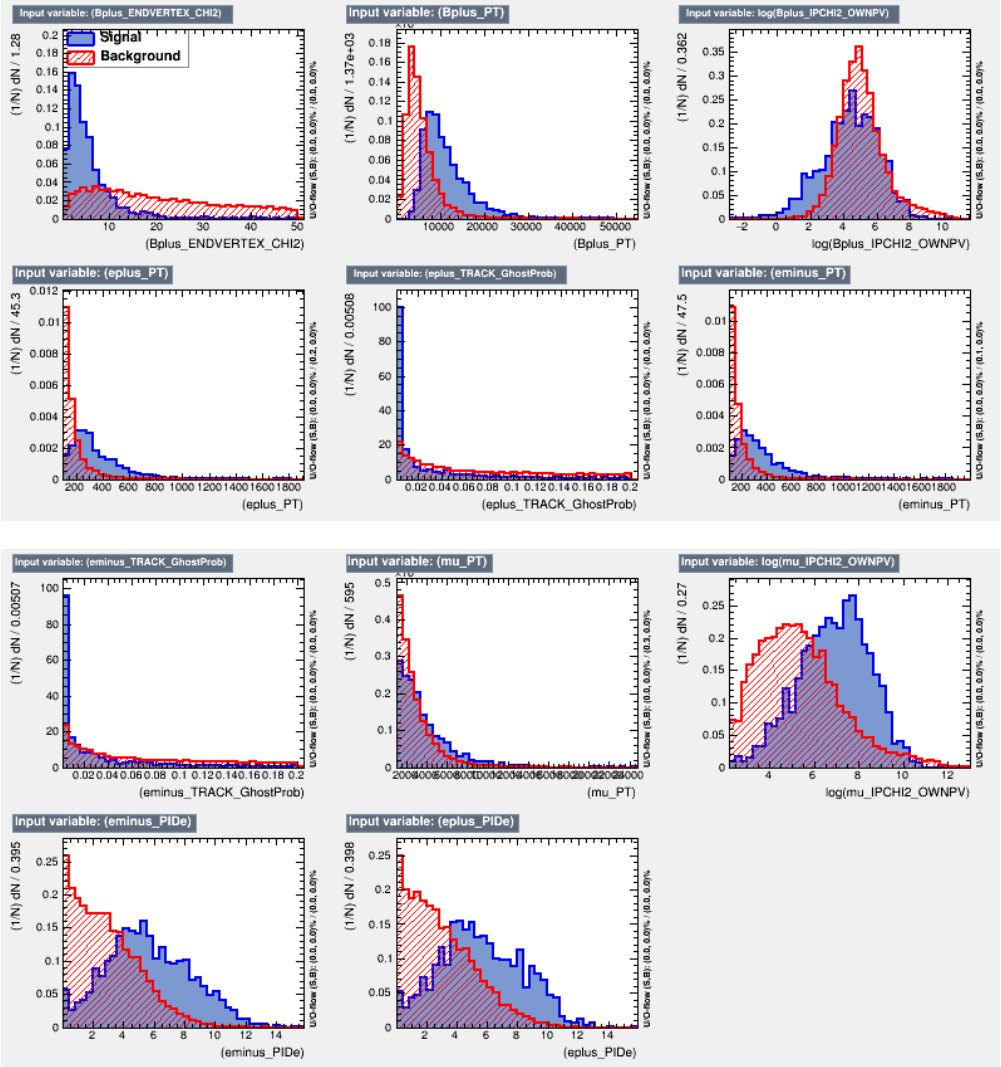

Figure 4.7: Comparison of the variables used in the Multivariate Analysis. In blue the signal (reweighted Monte Carlo sample) and in red the background (background data sample).

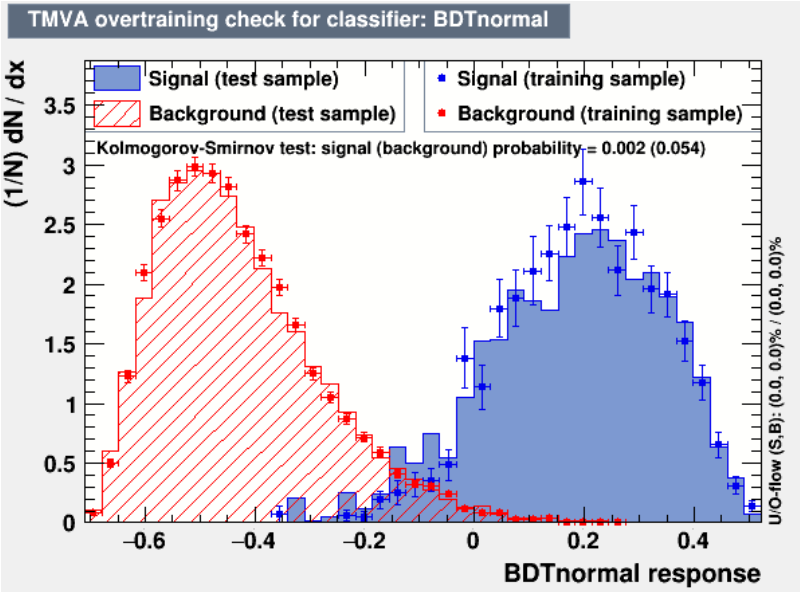

Figure 4.8: The BDT response with the Monte Carlo signal in blue and the background in red. Training and testing samples are both drawn, with training as points with error bars and testing as bar chart.

4.6 Applying the BDT

After testing and training of the BDT it is now used on data to gain a signal data sample. The best cut value must be obtained. From the BDT response seen in figure 4.8 a value between -0.1 and 0.3 seems plausible since for -0.1 the background is as high as the signal and almost no signal events are lost, and for 0.3 all background is eliminated and only the signal is left but merely half of it. The optimal value lies somewhere in between these values and is determined with the figure of merit

$$\frac{signal}{\sqrt{signal + background}}.$$

The signal and background values are obtained from the yields of a fit on the Δm variable for different BDT cuts. The fit is the same fit as in section 4.4.1 used to sweight the data of the control channel except that no gaussian is fitted since there is no second peak at 80 MeV now. The peak was most likely lost due to the BDT cuts. The fit consists of a Crystall Ball function for the signal and a square root function for the background. To now determine the best cut value the figure of merit is calculated for events between a BDT cut of 0.1 and 0.3 with a stepping of 0.01. The resulting figure of merits are plotted in figure 4.9 for both Mag Up and Mag Down. The separation in Mag Up and Mag Down has no physical meaning it is just convenience since the data sample is gathered in separate files for Mag Up and Mag Down. To gain statistical Independence and independent non biased cut results this is made on the Mag Up sample and the optimal value is then used on the Mag Down sample and vice versa. As seen in the figure there is no significant peak for the figure of merit. This has several reasons, for one is their no clear peak of the signal at the value there is just noise. Second is the fit function not always converging correctly. As solution to this Problem a BDT cut of 0.3 was made since it offers the best backgound elimination according to figure 4.8. As a better model for the figure of merit the a figure of merit established by Giovanni Punzi [17] could be used. Instead of the signal as discriminating value it uses the efficiency, which in the case of this thesis is gathered by the Monte Carlo sample. But due to time constraints this could not be finished before writing this thesis.

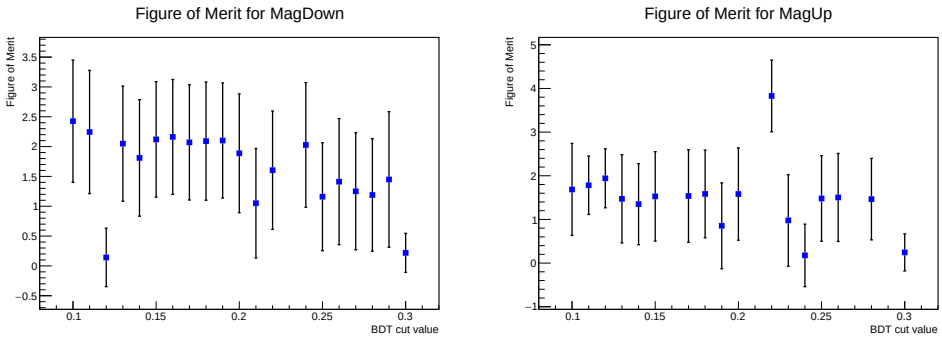

(a) Graph with the figure of merit over the BDT cut value for the Mag Down data.

(b) Graph with the figure of merit over the BDT cut value for the Mag Up data.

Figure 4.9: The Graphs with the measured figure of merit over the BDT cut value on data. The measured fom values are blue dots.

4.7 Selection Result

At last the a fit on the data sample is made to extract the signal yield. For this the now with a BDT cut optimized Tuples are merged together and the signal region is again fitted with a Crystal Ball function for the signal and a square root function for the Background. The two Crystal Ball functions share the same μ since they both describe the same peak. The complete fit function has now the form of this:

$$\begin{aligned} F_{full} = Y_{sig} \cdot (&frac \cdot CB(x; \alpha_1, n_1, \mu, \sigma_1) \\ &+ (1 - frac) \cdot CB1(x; \alpha_2, n_2, \mu, \sigma_2)) \\ &+ Y_{BG} \cdot sqf(x; a, b) \end{aligned}$$

At first the Monte Carlo sample is fitted with a double CB function for the Signal and a square root function for the Background. The used fit is a unbinned likelihood fit. This is done first to obtain a correct fit function and second for the fit parameters of the Mont Carlo sample. The μ parameter was fixed on 138 MeV as well as the start parameter b for the square root function on 60 MeV, for a convergence of the fit. The fit on Monte Carlo can be seen in figure 4.10. Now the same fit was made on the data sample with the fit parameters gained from the Monte Carlo sample. The only free parameters were the yields, σ_2 of the second Crystall Ball function and b the slope of the sqf.

The Signal yield for the Monte Carlo is

$$Yield_{Signal,MC} = 896 \pm 14,$$

taken from figure 4.10. And the signal yield for the data channel is

$$Yield_{Signal,data} = 21.7 \pm 17.2,$$

as seen in figure 4.11. For the next step those two yields will be needed for the calculation of the selection efficiency and afterwards the branching fraction of the $D^{*0} \to D^0 \to e^- e^+$ decay. Clearly seen is that the fit on data is not based on a data peak, which is also shown in the value of the signal yield with a large error of approximate 80 % of it's value. To verify this further the significance S is calculated using Wilk's theorem [] and the following formula,

$$S = sqrt2 \cdot (Min(log|L_{bg}|) - Min(log|L_{sig+bg}|))$$

where $Min(log|L_{bg}|)$ describes the minimum of the negative likelihood ratio of a fit with the background model only and $Min(log|L_{sig+bg}|)$ the minimum of the negative likelihood ratio of a fit with the background and signal model. The significance of this peak is

$$1.31\sigma$$

which underlines the poor result. Therefore a Branching ratio can not be determined from this signal yield, instead a upper limit will be approximated using a profile likelihood (PL) function [18]. The PL generally describes a concentration of parameters which are used to maximize the profile likelihood function. The profile likelihood ratio is used to gain a confidence interval for the used fit. It uses a Gaussian shape to estimate the confidence interval. The confidence level for this interval is 95 %.
As a result a upper limit of the confidence interval was taken. It correspond to the confidence of the yield and is

$$Y_{PL} = 48.9$$

with a confidence level of 95 %.

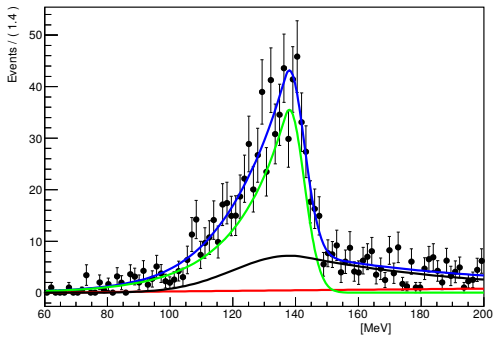

Fit parameters :

$$
\begin{aligned}
Y_{Signal} &= 896 \pm 14 \\
Y_{Background} &= 40.9 \pm 9.4 \\
frac &= 0,645 \pm 0.014 \\
\alpha_1 &= 0.296 \pm 0.026 \\
n_1 &= 118 \pm 13 \\
\sigma_1 &= 4.8 \pm 2.2 \\
\alpha_2 &= -0.317 \pm 0.035 \\
n_2 &= 106.0 \pm 4.3 \\
\sigma_2 &= 18.0 \pm 1.5 \\
a &= 0.93 \pm 0.12
\end{aligned}
$$

Figure 4.10: On the left the Fit of the Monte Carlo which is used to gain the signal yields and on the right the fit parameters obtained by the fit. The full fit function is shown in blue, the contribution of the first Crystall ball function in green, the second Crystall Ball function in black and the square root function in red.

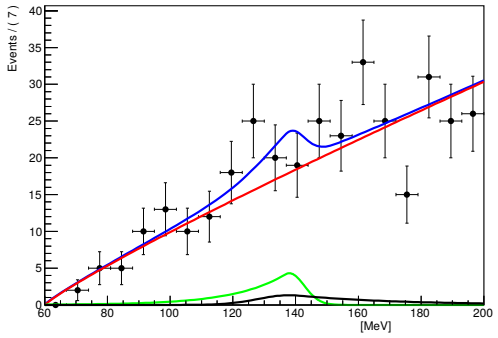

Fit parameters :

$$
\begin{aligned}
Y_{Signal} &= 21.7 \pm 17.2 \\
Y_{Background} &= 320 \pm 24 \\
\sigma_2 &= 9.99 \pm 9.87 \\
a &= 0.89 \pm 0.11
\end{aligned}
$$

Figure 4.11: On the left the Fit of the dataset which is used to gain the signal yields and on the right the fit parameters obtained by the fit. The full fit function is shown in blue, the contribution of the first Crystall ball function in green, the second Crystall Ball function in black and the square root function in red.

5 Determining the Branching Fraction

This Chapter describes the Calculation of the Branching Fraction. First the efficiency of the used cuts is determined by using the Monte Carlo sample and then the Branching Fraction is calculated.

5.1 Selection Efficiency

The Selection efficiency describes the ratio of signal events which are reconstructed and pass the signal selection to all signal candidates. To Calculate the Efficiency of the cut, the Monte Carlo sample is used, since the number of simulated decays is known which can not be said about the data. As number of final Monte Carlo event the yield of the signal in figure 4.10 is taken. The Monte Carlo was selected equally to the data channel, therefore the efficiency of the selection will be the same. For the efficiency ε the ratio between the generated and final signal events is determined.

$$\varepsilon = \frac{N_{end}}{N_{generated}}$$

with $N_{generated} = 4 \cdot 10^6$ events and $N_{end} = 896 \pm 14$ events it follows to

$$\varepsilon = (224 \pm 4) \cdot 10^{-6}.$$

5.2 Branching Fraction

With the known efficiency and the estimate for an Upper limit from the profile likelihood the Branching Fraction $\mathcal{B}(D^{*0} \to D^0 e^- e^+)$ can be calculated using the following formula

$$\mathcal{B}(D^{*0} \to D^0 e^- e^+) = \frac{N_{D^{*0} \to D^0 e^- e^+}}{2\sigma_{b\bar{b}} \cdot f_{b\to\mu\nu} \cdot \varepsilon \cdot \mathcal{B}(B^+ \to D^{*0}\mu\nu) \cdot \mathcal{B}(D^0 \to K^+\pi^-) \cdot \mathcal{L} \cdot \zeta}$$

where $\sigma_{b\bar{b}}$ is the cross section of the decay, N is the number of events, $f_{b\to\mu\nu}$ is the Probability of a b quark going into a $\mu\nu$, ε is the efficiency gathered from the Monte Carlo in section 5.1 and the $\mathcal{B}$'s are the Branching Fraction

of the observed Decays, which values are taken from [19]. The Number of events $N_{D^{*0}\to D^0 e^- e^+}$ is gathered by the upper limit estimated in the previous chapter. ζ is the relative geometric acceptance of the simulation. It resembles the fact, that not all decays are in range for the detector.

$$\begin{aligned}
\sigma_{b\bar{b}} &= 500\mu b \\
f_{b\to\mu\nu} &= 32\% \\
\varepsilon &= (224 \pm 4) \cdot 10^{-6} \\
\mathcal{B}(B^+ \to D^{*0}\mu\nu) &= (5.69 \pm 0.19)\% \\
N_{D^{*0}\to D^0 e^- e^+} &= 48.9 \\
\mathcal{B}(D^0 \to K^+\pi^-) &= (3.88 \pm 0.05)\% \\
\mathcal{L} &= 1.55\ fb^-1 \\
\zeta &= 15.8\ \%
\end{aligned}$$

Using all those values the Branching Fraction can be calculated to:

$$\mathcal{B}(D^{*0} \to D^0 e^- e^+) = (2.52 \pm 0.05_{stat}) \cdot 10^{-3}$$

Only errors gained from the fit models are taken into account here. This means the error of the efficency. Errors of the branching fractions are regarded as systematic uncertainty and discussed in the next chapter.

6 Systematic Uncertainty

A complete analysis on the systematic uncertainties is out of scope for this thesis. Nevertheless an Overview is given and the dominating factors are estimated whereas small ones are just shortly discussed.

One contribution of systematic uncertainty comes from the fit model. Since the fit is insufficient to describe the data completely. To now quantify this impact all fit parameters are left to float except for the background shape and the fraction of the Crystal Ball functions. The difference in signal yield from the fits is taken into account and correspond to a relative uncertainty of 3.2 %.

The uncertainty of simulated data and real data is also regarded as a systematic error. Even though the simulation was reweighted to match the control channel, the reweight only took place on one variable and there was still a noticeable difference in some values. An approximate estimate of this uncertainty was made by using the difference of the reweighted and unweighted Monte Carlo efficiencies. This results in an uncertainty of 1.1 %. For a better estimation the binning of the reweight could be varied or other variables could be used as reweighting variable.

The contribution of the used branching fractions plays a major role as systematic uncertainty. Their are two branching fractions used in this thesis their uncertainties are coming from [19]. Their contribution to the systematic uncertainty is large considering the other above calculated

Source	Relative Uncertainty [%]
Fit model	3.2
Simulation	1.1
$\mathcal{B}(B^+ \to D^{*0}\mu\nu)$	3.3
$\mathcal{B}(D^0 \to K^+\pi^-)$	1.29
Quadratic Sum	4.8

Table 6.1: Summary of all regarded contributions to the systematic uncertainty.

uncertainties with 3.3 % and 12.9 % respectively.

As a big source of uncertainty the preselection should be taken into account. Since the efficiency of the Monte Carlo sample is low it should be considered that there is some fault in the preselection. To take it into account a different preselection could be made and the difference of the resulting branching fraction could be made. Due to time constraints and the need to redo the complete chapter 4 for an analysis of this effect, this was not performed.

The total uncertainty is estimated to be 4.9 %. And thus more than double the relative statistical error of 1.8 %.

7 Summary and Outlook

In this thesis the upper limit for the branching fraction of the decay $D^{*0} \to D^0 e^- e^+$, using data samples from the LHCb experiment from the year 2016. The data was taken with a center-of-mass energy of $sqrts = 13\ TeV$ and an integrated luminosity of $1.55 fb^-1$.
To reduce the vast amount of combinatorial background the focus of this analysis was reducing this and giving a potential background channel for further analysis of Dark Photons in this Decay. In the case of this thesis the background was omnipresent and even with a multivariate analysis was still the only visible data. Since a signal was not seen a upper limit for the branching fraction was estimated by using profile likelihood ratio. The result is an upper limit for the branching ratio of

$$\mathcal{B}(D^{*0} \to D^0 e^- e^+) < (2.52 \pm 0.05_{stat.} \pm 0.12_{syst.}) \cdot 10^{-3}$$

where the upper limit for number of events is

$$N_{signal} = 48.9$$

which corresponds to a confidence level of 95 %. From [9] an estimation for the ratio of the branching fraction of this decay to the deacy $D^{*0} \to \gamma$ was made. This results in $\mathcal{B}(D^{*0} \to D^0 e^- e^+) = 2.4 \pm 0.2 \cdot 10^{-3}$. Which is in good estimation of the given result. The measurement in this thesis was dominated by the systematic uncertainty as seen in table 6.1, as well as a dominant background as seen in figure 4.11. In this thesis the efficiency of the Monte Carlo sample was low compared to other bachelor theses, therefor a fault in the preselection or the multivariate analysis can not be excluded. This could be a source for the dominant background and should be regarded in further analysis.

A Appendix

A.1 Reweighted Monte Carlo plots

Here are all missing plots of the reweight of the Monte Carlo sample.

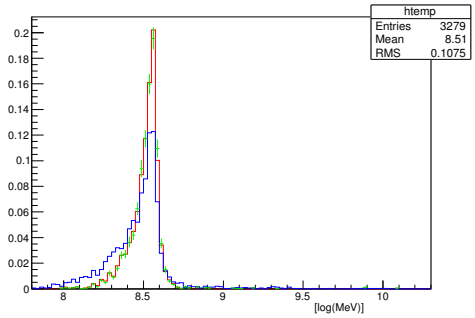

(a) log(B^+ corrected mass)

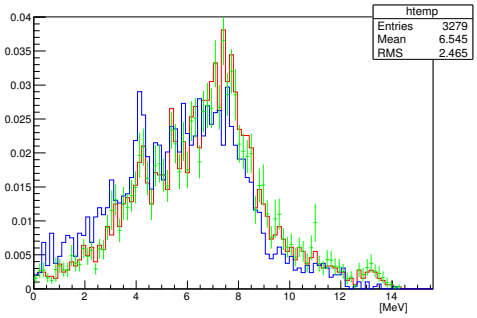

(b) μPID_{mu}

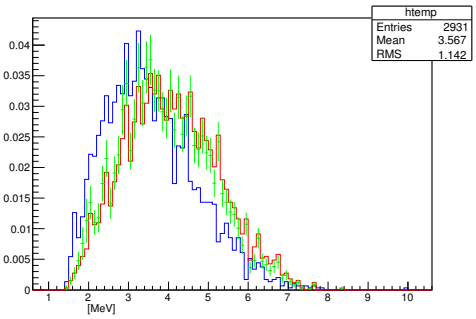

(c) Maximum IP_{χ^2} of the electrons.

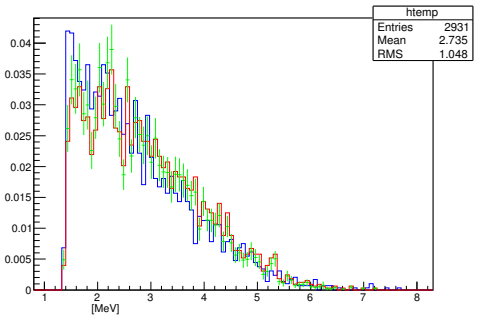

(d) Minimum IP_{χ^2} of the electrons

Figure A.1: Comparison of the reweighted Monte Carlo in green with the Monte Carlo before reweighting in blue and the sweighted data in red.

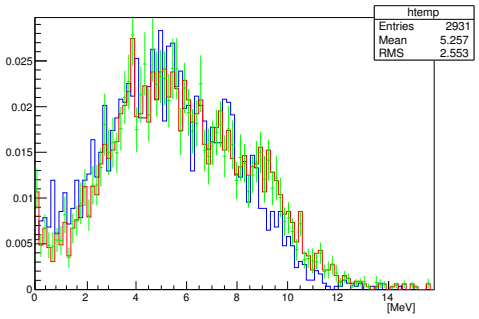

(a) $e^{+}PID_{e}$

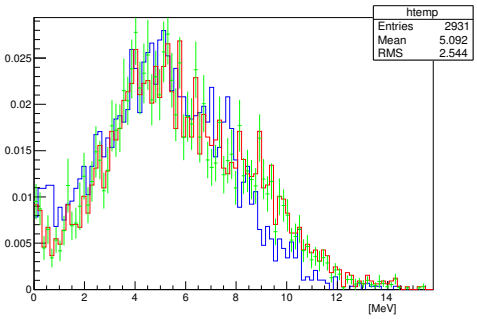

(b) $e^{-}PID_{e}$

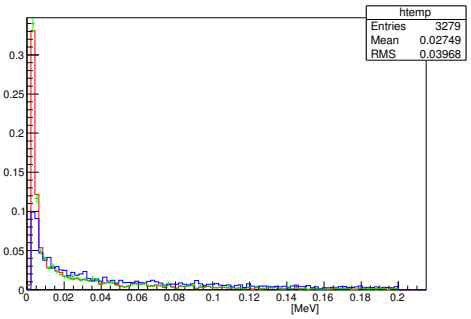

(c) e^{-} ghost probability

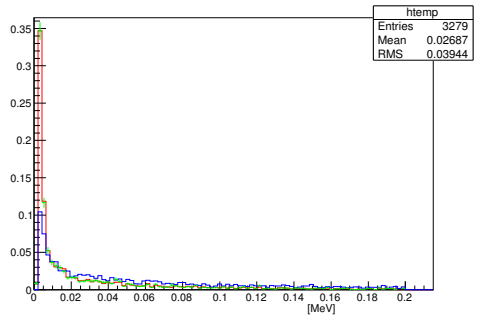

(d) e^{+} ghost probability

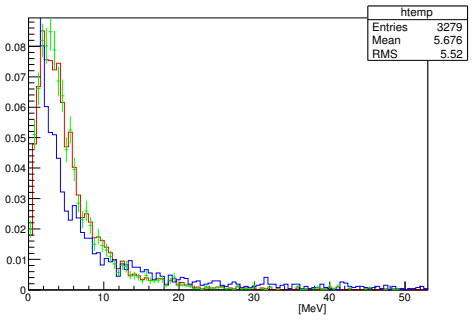

(e) $B^{+}vertex\chi^{2}$

Figure A.2: Comparison of the reweighted Monte Carlo in green with the Monte Carlo before reweighting in blue and the sweighted data in red.

B Bibliography

[1] Einstein, A. and Berger, N. *The World As I See It*. Philosophical Library/Open Road, 2011.

[2] F. Zwicky. Die Rotverschiebung von extragalaktischen Nebeln. *Helvetica Physica Acta*, 6:110–127, 1933.

[3] The LIGO Scientific Collaboration and the Virgo Collaboration. Observation of gravitational waves from a binary black hole merger. 2016.

[4] Mark Thomson. *Modern particle physics*. Cambridge University Press, 2013.

[5] Wikipedia and Wikipedia user AnonMoos. Standard_model_of_elementary_particles. https://upload.wikimedia.org/wikipedia/commons/archive/0/00/20130622193522%21Standard_Model_of_Elementary_Particles.svg, 2013. Visited on 07.02.2017.

[6] The LHCb collaboration. Amplitude analysis of $B^+ \to J/\psi\,\phi K^+$ decays. 2016.

[7] The LHCb collaboration . Observation of $J/\psi\ \rho$ resonances consistent with pentaquark states in $\Lambda_b^0 \to J/\psi\, K^-\rho$ decays. 2015.

[8] The ATLAS Collaboration. Observation of a new particle in the search for the standard model higgs boson with the atlas detector at the lhc. 2012.

[9] Philip Ilten and Jesse Thaler and Mike Williams and Wei Xue. Dark photons from charm mesons at LHCb. 2015.

[10] Cern. Cern-accelerator-complex. http://te-epc-lpc.web.cern.ch/te-epc-lpc/machines/lhc/general.stm, 2016. Visited on 22.02.2017.

[11] Rolf Lindner. "LHCb layout_2. LHCb schema_2". LHCb Collection.Visited on 17.02.2017, Feb 2008.

[12] Paul Seyfert. Tracking strategies used in lhcb. https://twiki.cern.ch/twiki/bin/view/LHCb/LHCbTrackingStrategies, 2012. Visited on 07.03.2017.

[13] Daniel Baitinger. Measurement of the branching ratio of the decay $B^+ \to J/\psi K^{*+}$ at the LHCb experiment. Bachelorarbeit, Universität Heidelberg, 2016.

[14] Muriel Pivk and Francois R. Le Diberder. sPlot: A statistical tool to unfold data distributions. *Nucl.Instrum.Meth.*, A555:356–369, 2005.

[15] Tomasz Skwarnicki. *A study of the radiative cascade transitions between the Upsilon-prime and Upsilon resonances*. PhD thesis, Institute of Nuclear Physics, Krakow, 1986. DESY-F31-86-02.

[16] A. Hoecker, P. Speckmayer, J. Stelzer, J. Therhaag, E. von Toerne, and H. Voss. Tmva - toolkit for multivariate data analysis. 2007.

[17] Giovanni Punzi. Sensitivity of searches for new signals and its optimization. 2003.

[18] Gioacchino Ranucci. The profile likelihood ratio and the look elsewhere effect in high energy physics. 2012.

[19] K. A. Olive et al. Review of particle physics. *Chin. Phys.*, C38:090001, 2014. and 2015 update.

[20] Paul André Günther. Measurement of the branching fraction of the rare decay $B^+ \to K^{*+}\mu^+\mu^-$ exploiting the $K^{*+} \to K^+\pi^0$ decay at the LHCb experiment. Bachelorarbeit, Universität Heidelberg, 2015.

[21] Ralf Klemt. Bestimmung des Verzweigungsverhältnisses des Zerfalls $B_s^0 \to \mu\mu f_0$ am LHCb-Experiment. Bachelorarbeit, Universität Heidelberg, 2014.

C Acknowledgment

At First I like to thank everyone who supported me during the last few months and especially for the last few weeks. A big thanks for my supervisor Prof. Dr. Stephanie Hansmann-Menzemer for not only giving me the option to work in the LHCb group, but for also the great help with writing of this thesis. Another toast goes out to Prof. Dr. Klaus Reygers for being the second referee of this thesis.
Special thanks goes out to Dr. Michel De Cian, the adviser for my bachelor thesis. He always knew a solution to a problem and was always available when needed. Thank you Thomas Nikodem and Jascha Grabowski for helping me out in a lot of problems and for sharing the bureau with me. Especially in the last weeks you were always helpful and had the right solutions at hand. I have learned a lot in my time here.
At last I want to thank all my family and friends for all their support and for being the help in all things not study related. Moritz Fäßler, Ludwig Weyl, Alex Schoedel, Robin Geiger, Max Lachmann, Davor Irsevic, Lukas Bange, Kilian Dietrich, Patrick Friebel, Jan Kilinc and Max Ellinger.Thank you all for making the past special and unforgettable.
Unforgettable is my beloved girlfriend, whom not only supported me for all my time writing this thesis she also acknowledged to my sanity by forcing me to not always write this Thesis by night. Thanks for helping me through this rough time.
Am meisten jedoch möchte ich meiner Familie und vor allem meinen Eltern danken. Ihr habt mich bisher bei all meinen Vorhaben unterstützt und ihr seit in allen Lebenslagen für mich dagewesen. Ich bin euch für alles unendlich dankbar.

Erklärung

Ich versichere, dass ich diese Arbeit selbstständig verfasst und keine anderen als die angegebenen Quellen und Hilfsmittel benutzt habe.

Heidelberg, den 13.März

Richard Kaiser